

Visual Input to the *Drosophila* Central Complex by Developmentally and Functionally Distinct Neuronal Populations

Highlights

- We identify a *Drosophila* brain circuit providing visual input to the central complex
- Neuron classes in this circuit are organized based on progenitor origin, or lineage
- Two lineages (DALcl1/2) provide parallel input to ellipsoid body ring neurons
- DALcl1 and 2 project to discrete domains and transmit different visual information

Authors

Jaison Jiro Omoto,
Mehmet Fatih Keleş,
Bao-Chau Minh Nguyen,
Cheyenne Bolanos,
Jennifer Kelly Lovick, Mark Arthur Frye,
Volker Hartenstein

Correspondence

frye@ucla.edu (M.A.F.),
volkerh@mcdb.ucla.edu (V.H.)

In Brief

Omoto et al. identify the anterior visual pathway, a circuit in the *Drosophila* brain consisting of neurons, the structure and function of which are defined by their progenitor origin, or lineage. This circuit is responsible for relaying information from the visual system to the central complex, an important region for visually guided behavior.

Visual Input to the *Drosophila* Central Complex by Developmentally and Functionally Distinct Neuronal Populations

Jaison Jiro Omoto,^{1,3} Mehmet Fatih Keleş,^{2,3} Bao-Chau Minh Nguyen,¹ Cheyenne Bolanos,¹ Jennifer Kelly Lovick,¹ Mark Arthur Frye,^{2,4,*} and Volker Hartenstein^{1,*}

¹Department of Molecular, Cell and Developmental Biology, University of California, Los Angeles, Los Angeles, CA 90095, USA

²Department of Integrative Biology and Physiology, University of California, Los Angeles, Los Angeles, CA 90095, USA

³Co-first author

⁴Lead Contact

*Correspondence: frye@ucla.edu (M.A.F.), volkerh@mcdb.ucla.edu (V.H.)

<http://dx.doi.org/10.1016/j.cub.2017.02.063>

SUMMARY

The *Drosophila* central brain consists of stereotyped neural lineages, developmental-structural units of macrocircuitry formed by the sibling neurons of single progenitors called neuroblasts. We demonstrate that the lineage principle guides the connectivity and function of neurons, providing input to the central complex, a collection of neuropil compartments important for visually guided behaviors. One of these compartments is the ellipsoid body (EB), a structure formed largely by the axons of ring (R) neurons, all of which are generated by a single lineage, DALv2. Two further lineages, DALcl1 and DALcl2, produce neurons that connect the anterior optic tubercle, a central brain visual center, with R neurons. Finally, DALcl1/2 receive input from visual projection neurons of the optic lobe medulla, completing a three-legged circuit that we call the anterior visual pathway (AVP). The AVP bears a fundamental resemblance to the sky-compass pathway, a visual navigation circuit described in other insects. Neuroanatomical analysis and two-photon calcium imaging demonstrate that DALcl1 and DALcl2 form two parallel channels, establishing connections with R neurons located in the peripheral and central domains of the EB, respectively. Although neurons of both lineages preferentially respond to bright objects, DALcl1 neurons have small ipsilateral, retinotopically ordered receptive fields, whereas DALcl2 neurons share a large excitatory receptive field in the contralateral hemifield. DALcl2 neurons become inhibited when the object enters the ipsilateral hemifield and display an additional excitation after the object leaves the field of view. Thus, the spatial position of a bright feature, such as a celestial body, may be encoded within this pathway.

INTRODUCTION

The central complex (CX) is an evolutionarily conserved domain in the insect brain that has a highly ordered, modular neuronal architecture. In *Drosophila*, it comprises several compartments that are situated across the brain midline, including (from anterior to posterior), the ellipsoid body (EB), fan-shaped body (FB) with noduli (NO), and protocerebral bridge (PB) [1–3]. The ellipsoid body is flanked laterally by two compartments of the lateral complex, the bulb (BU) and lateral accessory lobe (LAL), which act as portals for input to and output from the central complex.

Numerous anatomical, functional, and genetic studies conducted in the past suggest that the central complex is involved, among other functions, in the control of motor output and spatial orientation. Stimulation of the CX alters a large number of behaviors that require fine motor control, including stridulation, walking, and escape [4, 5]. Genetic lesions of the CX affect walking and flight [6, 7]. Silencing specific classes of ring neurons innervating the ellipsoid body of the CX causes deficits in visual place learning and spatial orientation memory in *Drosophila* [8, 9]. Along these lines, functional imaging studies in behaving flies suggest that populations of columnar neurons in the CX encode the fly's spatial orientation relative to its environment [10], suggesting that the CX could play a navigational role similar to that one of the hippocampus and entorhinal cortex in mammals [11].

Similar to the mushroom body, another highly structured neuropil domain of the insect brain known for its pivotal function in olfactory learning and memory, the central complex does not receive direct input from peripheral sense organs. Processed sensory information is relayed from the primary olfactory center (antennal lobe) to the mushroom body and superior protocerebrum via antennal lobe projection neurons. These anatomically and functionally specialized neurons are derived from four developmentally defined classes, so-called lineages [12, 13]. A lineage comprises all neurons produced by a single neural progenitor (neuroblast). The fly brain is generated by approximately 100 pairs of such neuroblasts, each of which is defined by a unique pattern of gene expression that dictates the morphology and function of the cells within the lineage [14]. Its lineage-based composition provides great conceptual and

technical advantages to analyze the structure and development of the antennal lobe projection in great detail, making this input pathway one of the pre-eminent model systems to study the genetic mechanism controlling the assembly of a central brain circuit [15, 16].

By comparison to the antennal lobe input pathway toward the mushroom body, very little is known about the circuitry providing input to the *Drosophila* central complex. It must receive input from the visual system; dendrites of ellipsoid body ring (R) neurons, located in the bulb, are sensitive to visual stimuli and form a retinotopically ordered arrangement [17]. In other insects, neurons conducting visual information from the optic lobe to the CX have been characterized, using anatomical and electrophysiological methods, in considerable detail [18]. This circuit, called the sky-compass pathway, is thought to encode skylight cue information relevant for navigation, such as the spatial position of bright celestial bodies, the pattern of polarized skylight, or the sky's spectral gradient. It is a pathway consisting of multiple layers; neurons of the optic lobe medulla project to a known domain of visual input in the central brain called the anterior optic tubercle (AOTU). From there, information is relayed by another neuronal population to the bulb, the input domain of tangential neurons which arborize in the central body lower division (homologous to *Drosophila* R neurons and ellipsoid body) [19–24].

In this paper, we have investigated the visual input pathway to the central complex in *Drosophila*. Which, if any, lineages form the “building blocks” of this pathway? Does the lineage principle guide the structural connectivity and thus the function of neuronal circuit elements within this pathway? Using clonal analysis, we and others previously identified the projection pattern for the majority of neuroblast lineages in the *Drosophila* brain [25–28]. This analysis revealed that R neurons of the ellipsoid body are derived from a single paired lineage (DALv2). Two additional lineages (DALc1 and 2) were identified; similarly to neurons in the sky-compass pathway, they project from the AOTU to the bulb, and we thus call them tuberculo-bulbar (TuBu) neurons. Identification of Gal4 drivers that reflect the projection pattern of neurons within these lineages allowed us to demonstrate a parallel pattern of topographically ordered connectivity within this pathway. Double labeling and GFP reconstitution across synaptic partners (GRASP) demonstrates that TuBu neurons provide direct input to R neurons. Two-photon calcium imaging of TuBu neuron presynaptic terminals further corroborates this notion; TuBu neuron outputs from DALc1, which predominantly innervate the superior domain of the bulb, exhibit similar response properties as R neuron dendrites from the same region, based on previous studies [17]. However, DALc2 TuBu neuron outputs, which predominantly innervate the inferior domain of the bulb, do not respond in the same fashion, demonstrating that the lineage principle determines not only the structure but also the function of neuronal populations.

RESULTS

Discrete Neural Lineages Form Input Pathways of the Ellipsoid Body

The pathway providing input from the optic lobe to the ellipsoid body, called the anterior visual pathway (AVP) in the following

(Figure 1A), represents a circuit whose central part is formed by the neurons of three lineages. As known from previous works and summarized above, R neurons of lineage DALv2 project from the bulb to the ellipsoid body. Cell bodies of this lineage are located in the anterior brain cortex, surrounding the spur of the mushroom body. The bulb receives the short, proximal neurites of DALv2 neurons; DALv2 axons form a fiber tract, termed the anterior lateral ellipsoid body tract (LEa), which extends medially toward the EB (Figure 1B) [2, 29].

We identified two hemilineages, DALc1d and DALc2d, which interconnect the bulb with the AOTU via TuBu neurons (Figures 1C and 1D). The identified neurons resemble likely homologs, called tubercle-LAL type 1 neurons (TuLAL1 neurons), from the sky-compass pathway [18]. The AOTU consists of a large, spherical medial compartment (AOTUm), to which two smaller domains (intermediate AOTU [AOTUin] and lateral AOTU [AOTUi]) are attached [1] (Figure 1A). In many other insects, the AOTU is oriented such that the larger domain is located dorsally of the smaller domains and is therefore called the upper unit (AOTU-UU) and lower unit (AOTU-LU) or lower unit complex (AOTU-LUC), respectively. DALc1d TuBu neurons appear to have short, proximal processes in the lateral AOTU (AOTUi) and distal terminals in the superior (BUs) and anterior BU (BUa) (Figures 1C and 1E). DALc2d TuBu neurons innervate complementary regions, connecting the AOTUin with the inferior BU (BUi) (Figures 1D and 1E). We did not identify neurons projecting directly from the large AOTUm compartment to the CX.

Visual interneurons of the medulla provide input to the AOTUi and AOTUin via a thick fiber bundle, the anterior optic tract (AOT). Gal4 driver lines reveal several discrete subpopulations of such medullo-tubercular (MeTu) neurons with proximal dendrites extending in medulla layer m6–8 (Figures 1F and 1G) and distal axonal branches confined to the lateral and intermediate AOTU. Putative homologies between neurons of the AVP and the sky-compass pathway from other insects are summarized in Table 1.

By expressing reporter proteins specifically targeted to presynaptic terminals (*UAS-syt.GFP*) and postsynaptic membranes (*UAS-DenMark*) we can show that the AVP is directed from the medulla to the AOTU and, from there, toward the ellipsoid body. Thus, projections of DALv2 R neurons are mostly axonal in the EB and dendritic in the BU (Figure 1H). Likewise, projections of DALc1/2 TuBu neurons have mostly presynaptic, axonal sites in the bulb and postsynaptic, dendritic sites in the AOTU (Figure 1I). Proximal neurites of MeTu neurons in the medulla are exclusively dendritic; distal projections in the AOTU appear to possess intermingled presynaptic and postsynaptic sites (Figure 1J). Although the AVP is predominantly centripetal, the presence of dendritic and axonal signal in the centrifugal direction suggests potential feedback in this circuit.

R Neuron Subclasses of DALv2 Establish a Topographically Ordered Connectivity between the Bulb and Ellipsoid Body

Global markers for neuropil (antibodies against DN-cadherin [DNcad] or Bruchpilot [Brp]) in conjunction with specific Gal4 driver lines reveal more detail about the intricate anatomy and connectivity within the AVP. In the EB, five discrete domains

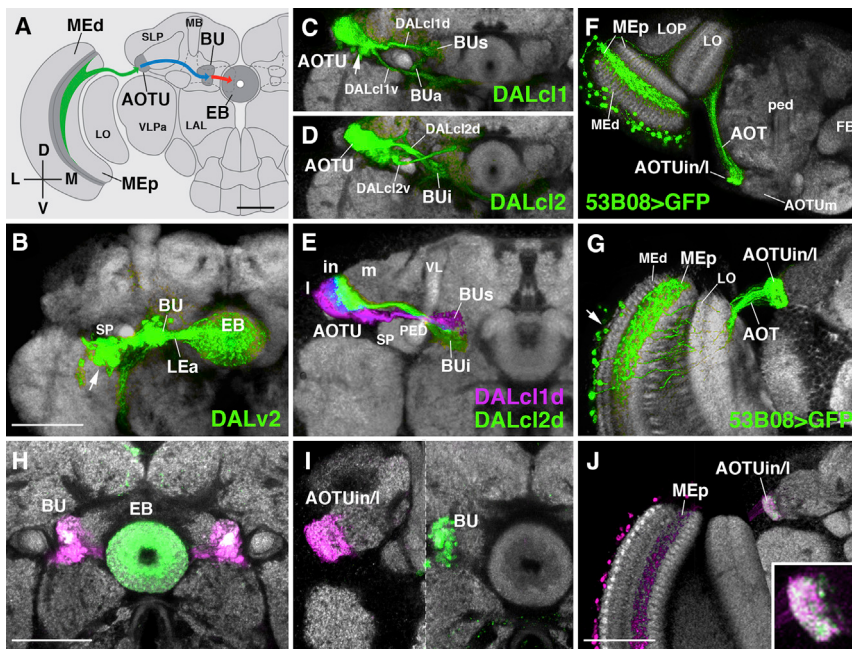


Figure 1. Discrete Lineages Constitute the Central Brain Components of the Anterior Visual Pathway

(A) Schematicized overview of the three-legged AVP. First leg (green) is from the optic lobe medulla to the anterior optic tubercle (AOTU). Second leg (blue) is from the AOTU to bulb (BU). Final leg (red) is from the bulb (BU) to the ellipsoid body (EB) of the central complex.

(B–J) Confocal z projections illustrating the anterior visual pathway (AVP) (frontal sections unless otherwise noted); adult brains labeled with anti-DN-cadherin (gray) and cell body clusters depicted by arrows.

(B–D) MARCM clones of secondary lineages DALv2, DALc1d, and DALc1d (green) (nomenclature from [26, 29]).

(B) DALv2 forms all R neurons of the EB (red leg in A), projecting from the BU to the EB via the anterior lateral ellipsoid body tract (LEa).

(C and D) DALc1d and DALc1d form TuBu neurons (blue leg in A). Two tract components emanate from each neuroblast clone, a dorsal (DALc1d/2d) and a ventral (DALc1d/2v) component, which we conclude are hemilineages. The dorsal, not ventral, hemilineages form the TuBu neurons.

(E) Isolation and registration of DALc1d/2 dorsal hemilineages (see [Experimental Procedures](#); DALc1d, magenta; DALc1d/2d, green). Neurites of DALc1d project from the lateral domain of the AOTU (AOTU) to the superior domain of the bulb (BUs), and DALc1d/2d projects from the intermediate domain of the AOTU (AOTU) to the inferior domain of the bulb (BUi). We did not identify neurons projecting from the large medial domain of the AOTU (AOTU) to the bulb.

(F and G) Horizontal (F) and frontal (G) sections of R53B08-Ga4 (green) labeling medullo-tubercular neurons, projecting from the medulla to the AOTUin/l via the anterior optic tract (AOT) (green leg in A).

(H–J) Expression of presynaptic marker syt::GFP (green) and dendritic marker DenMark (magenta) in distinct legs of the AVP.

(H) R20A02-Ga4 labels most R neurons and shows enrichment of axonal output in the EB and dendrites in the BU.

(I) R48B06-Ga4 labels TuBu neurons and shows enrichment of output in the BU and dendrites in the AOTUin/l.

(J) R53B08-Ga4 demonstrates medullo-tubercular neurons are dendritic in the proximal medulla (MEp) but appears to have mixed dendritic and axonal specializations in the AOTUin/l (boxed inset).

LAL, lateral accessory lobe; LO, lobula; LOP, lobula plate; MB, mushroom body; MEd, distal medulla; PED, peduncle of the mushroom body; SLP, superior lateral protocerebrum; SP, spur of the mushroom body; VL, vertical lobe; VLPa, anterior ventrolateral protocerebrum. The scale bars represent 50 μm (A, C, D, and F), 50 μm (B, E, G, and J), and 50 μm (H and I).

can be distinguished based on different expression levels of DN-cadherin ([Figures 2A–C](#)). These comprise an inner posterior domain (EBip) and inner central domain (EBic) with low DNcad signal, an outer central domain (EBoc) with moderate DNcad signal, and an anterior domain (EBa) and outer posterior domain (EBop) with high signal. The bulb consists of three major domains defined by their position relative to the LEa fiber bundle formed by DALv2-derived R neuron axons. The superior and inferior domains of the bulb are located dorsally and ventrally of the LEa, respectively; the anterior bulb is attached to the lateral surface of the LEa at a position where it bends medially ([Figures 2A](#) and [2B](#)). DNcad labeling reveals the individual, large-input synapses, called microglomeruli, formed by R neuron dendrites ([Figure 2B](#), arrowheads).

We screened the expression patterns of several Gal4 driver lines that label subpopulations of R neurons [[30](#)]. This analysis, in conjunction with single-cell labeling using the multicolor flip-out method (MCFO) [[31](#)], reveals that the R domains of the ellipsoid body are connected in a topographically ordered pattern to the bulb, consistent with previous reports [[32](#)]. Previously unclassified R neurons innervating the anterior domain, which we call R5 ([Figures 2D–F](#)), and R2 neurons of the outer central domain ([Figures 2G–I](#)) have dendrites in the superior

bulb; other R neurons innervating the outer central domain are connected to the anterior bulb (R4m; [Figures 2J–L](#)). R neurons innervating the inner central and inner posterior domain possess dendrites in the inferior bulb (R3; [Figures 2M–O](#)).

We did not identify any R neurons that form axons in the outer posterior domain of the ellipsoid body. This domain, as well as the other domains of the EB, is innervated by two main classes of columnar neurons that interconnect the different compartments of the central complex, PB-EB-gall (“wedge”) neurons ([Figures 2P](#) and [2Q](#)) and PB-EB-NO (“tile”) neurons ([Figure 2R](#)) [[33](#)]. Both represent sublineages of four large type II lineages (DM1/DPMm1, DM2/DPMpm1, DM3/DPMpm2, and DM4/CM4) [[26, 34](#)], whose cell bodies are located in the posterior brain. Wedge neurons have proximal branches in the protocerebral bridge; from here, they extend forward, through the fan-shaped body, into the EB, where they presumably receive R neuron input. Collateral branches of wedge neurons project further forward into the gall of the LAL [[1, 33](#)] ([Figures 2P](#) and [2Q](#)); the LAL is a region thought to be relevant for locomotor output in insects [[35](#)]. Tile neurons have a more restricted projection to the outer posterior EB ([Figure 2R](#)) and therefore overlap extensively with wedge neurons, but not R neurons.

Table 1. Comparative Terminology for Central Complex Pathways

Putative Homologies in Other Insects	Drosophila Neuron Classification	Abridged Designation(s)	Subclasses	Lineage Designation
Transmedulla neurons, formerly line-tangential neurons	medullo-tubercular neurons	MeTu neurons	MeTu _l	optic lobe-derived
			MeTu _{il}	optic lobe-derived
			MeTu _{im}	optic lobe-derived
Tubercle-lateral accessory lobe neuron type 1 (TuLAL1 neurons)	TuBu neurons	TuBu	TuBu _s	DALcl1
			TuBu _a	DALcl1
			TuBu _i	DALcl2
Tangential neurons of the central body lower division (TL neurons)	R neurons	R neurons	R1, R2, R3, R4m, R4d	DALv2
			R5 (new designation—previously unclassified)	
Columnar neurons of the CBL type 1 (CL1 neurons)	protocerebral bridge-ellipsoid body-Gall neurons	PB-EB-gall (wedge neurons)		DM1/DPMm1, DM2/DPMpm1, DM3/DPMpm2, DM4/CM4
Columnar neurons of the CBL type 2 (CL2 neurons)	protocerebral bridge-ellipsoid body-noduli neurons	PB-EB-NO (tile neurons)		DM1/DPMm1, DM2/DPMpm1, DM3/DPMpm2, DM4/CM4

TuBu Neurons of DALcl1 and DALcl2 Form a Topographically Ordered Projection between the AOTU and Bulb

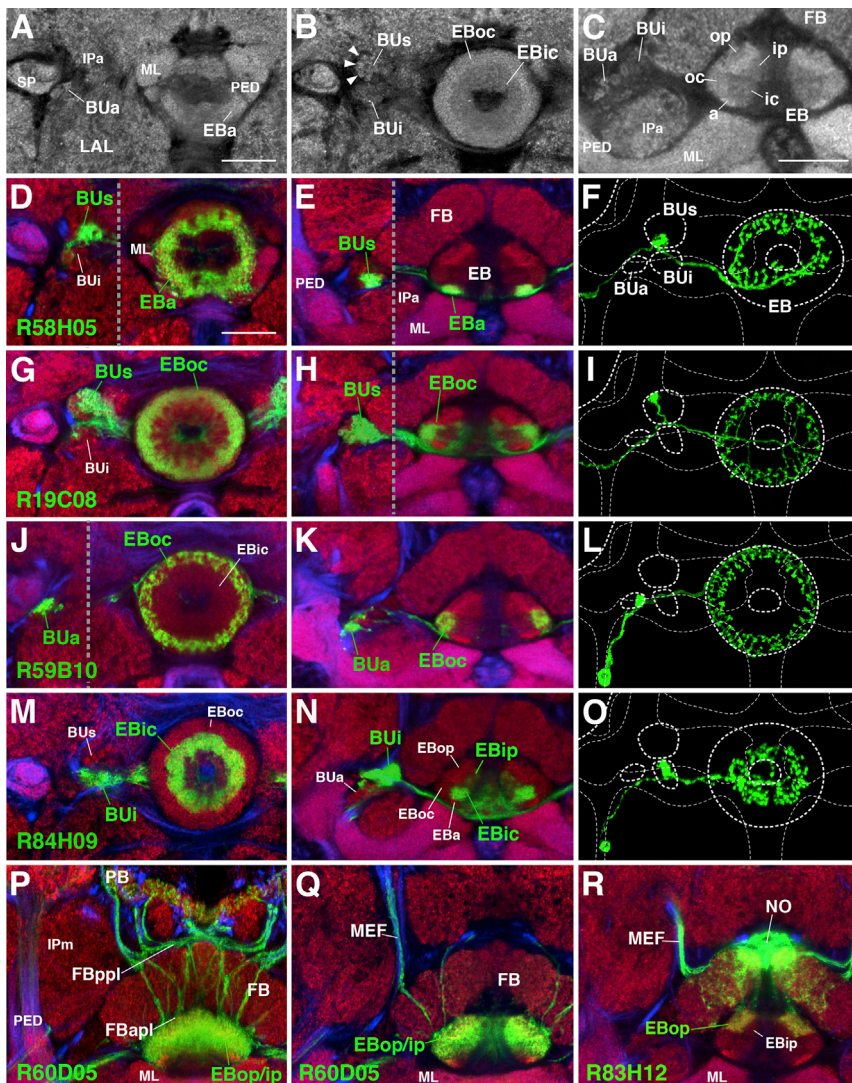
In view of the ordered connectivity between bulb and ellipsoid body, it stands to reason that neurons of DALcl1 and DALcl2, which connect the AOTU to the bulb, are also topographically organized. Based on DNCad expression, three subdomains (medial, intermediate, and lateral) can be defined for the AOTU [1]. Closer inspection of DNCad-labeled brains revealed that the intermediate domain is further subdivided into two narrow, vertical slices, named (from lateral to medial) AOTUiL and AOTUiM (Figures 3A and 3B). The lateral domain, AOTUiL, is divided into three finger-like processes (AOTUiLa, AOTUiLc, and AOTUiLp) that are most easily revealed in horizontal sections of the tubercle (Figure 3B).

We identified multiple Gal4 driver lines expressed in subpopulations of MeTu neurons and DALcl1- and 2-derived TuBu neurons whose projection is predominantly restricted to specific subdomains of the AOTU, additionally corroborated by MCFO-labeled single-cell clones. The DALcl1-derived TuBu subpopulation with axons terminating primarily in the superior bulb (TuBu_s) has dendrites enriched in all three processes of the lateral subdomain (AOTUiLa/c/p) and can be labeled by R88A06-Gal4 (Figures 3D–3F). TuBu neurons terminating in the anterior bulb (TuBu_a), also derived from DALcl1, actually exhibit dendrites filling the lateral slice of the intermediate AOTU subdomain (AOTUiL) (Figures 3G–3I). Dendrites of inferior bulb TuBu neurons (TuBu_i), derived from DALcl2, are concentrated in the medial intermediate subdomain (AOTUiM) and express R49E09-Gal4 (Figures 3J–3L). The parallel pathways connecting the AOTU with the bulb and ellipsoid body are schematically summarized in Figure 4.

MeTu neurons from the medulla (previously described [36] as medullar columnar 61 neurons [MC61]) also terminate in specific subdomains of the lateral and intermediate AOTU defined by the dendrites of TuBu neurons. The AOTUm receives input from the lobula (lobula columnar 10 [LC10]) [37]. Numerous driver lines expressed in MeTu neurons have been identified; three repre-

sentative examples are depicted in Figures 3M–3T. Dendrites fill predominantly layer m7, with sparser branches reaching up into m6 (the layer contacted by photoreceptors R7) and deeper into m8. The somata of some MeTu neurons are distributed throughout the dorsal half of the medulla cortex, as shown here for neurons innervating the AOTUiL domain (MeTu_{il}) (Figures 3Q and 3R) and the AOTUiM domain (MeTu_{im}) (Figures 3S and 3T). Cell bodies of other MeTu neurons, such as those innervating AOTUiL (MeTu_l) (Figures 3M and 3N), are spread out over the entire medulla. Single-cell clones of MeTu_l (R73C04-Gal4) reveal that the dendritic tree arborizes locally of the primary neurite and covers 10–15 contiguous medulla columns (Figures 3O–3O'). Therefore, this class of neurons collectively innervates the entire medulla, rather than each individual neuron doing so, identifying MeTu neurons as special subclasses of multicolumnar medullary visual projection neurons. Their cell body location and projection pattern are reminiscent of *Drosophila* transmedullary neurons but exhibit a single dendritic tree and, instead of targeting the lobula complex, directly project to the central brain [38].

Concomitant labeling of DALcl1 or DALcl2 TuBu neurons and DALv2 R neurons demonstrates that the endings of the former fully overlap with the proximal branches of the latter in the bulb (Figures 4B and 4C). Given the large size of the pre- and postsynaptic endings, forming microglomeruli of approximately 2 μm diameter, it was evident that individual R neuron dendrites were directly contacted by TuBu neuron axons. To provide further evidence for a direct synaptic contact, we carried out a GRASP analysis, in which the postsynaptic cells are expressing CD2-RFP and split-GFP11, whereas the presynaptic cells express split-GFP1–10. As shown in Figures 4D and 4E, a strong GRASP signal is detected specifically in the bulb within the expected target region. DALcl1-derived TuBu_s neurons innervate R2 neurons of EBoc with microglomerular dendrites in the superior bulb, whereas DALcl2-derived TuBu_i neurons innervate R3 neurons of EBic in the inferior bulb, confirming the presence of parallel, superior, and inferior bulb pathways.



(R) *R83H12-Gal4* labels PB-EB-NO (“tile”) neurons, which fill the outer posterior domain of the EB (EBop). FB, fan shaped body; FBapl and FBppl, anterior and posterior plexus of the fan shaped body; IPa and IPm, anterior and medial inferior protocerebrum; LAL, lateral accessory lobe; MEF, medial equatorial fascicle; ML, medial lobe of the mushroom body; NO, noduli; PB, protocerebral bridge; PED, peduncle of the mushroom body; SMP, superior medial protocerebrum; SP, spur of the mushroom body; VL, vertical lobe. The scale bars represent 25 μ m (A and B), 25 μ m (C), and 25 μ m (D–R).

Lineally Organized Input Channels to the Ellipsoid Body Form Parallel Neural Ensembles that Are Functionally Distinct

Previous studies utilizing pan-neuronal or R-neuron-specific (R2 and R4d) two-photon calcium imaging in the superior bulb demonstrated that a subpopulation of R neuron dendrites respond to visual features. Visually responsive dendritic microglomeruli typically exhibit ipsilateral receptive fields, bright (ON) selectivity, and vertical orientation tuning [17]. Our anatomical data demonstrate that TuBu neurons provide direct input to R neuron dendrites; we therefore tested the hypothesis that the microglomerular presynaptic terminals of TuBu neurons exhibit similar physiological properties as R neuron dendrites. We expressed the genetically encoded calcium indicator GCAMP6m

Figure 2. DN-Cadherin Domains and Single-Cell Labeling Define the Topology and Architecture of Ellipsoid Body Neurons

(A–C) High-magnification frontal (A and B) and horizontal (C) z projections of the bulb and ellipsoid body neuropil labeled by anti-DN-cadherin (gray) reveals three distinct domains in the bulb and five distinct domains in the ellipsoid body.

(A) Anterior frontal section reveals the anterior bulb (BUa) and the anterior domain of the EB (EBa).

(B) Intermediate frontal section reveals the superior (BUs) and inferior (BUi) domains of the bulb and the outer central (EBoc) and inner central (EBic) domains of the EB. Arrowheads designate bulb microglomeruli.

(C) Horizontal section through the EB canal reveals all five EB domains.

(D–O) Gal4 drivers that label distinct R neuron subclasses defined by axon morphology and topology within the BU and EB. Each row represents a distinct Gal4 driver; first and second columns are frontal and horizontal sections labeled with 10xUAS-mCD8::GFP, respectively. Gray hatched lines denote regions of interest that are not within the same plane. Neuropil labeled with anti-DN-cadherin (red) and axon tracts by anti-neuroglian (blue) is shown. Third column is a single-cell clone generated by MCFO using the same Gal4 (see Experimental Procedures); white hatched lines outline neuropil compartments from the same fly.

(D–F) *R58H05-Gal4* (R5; BUs to EBa).

(G–I) *R19C08-Gal4* (R2; BUs to EBoc).

(J–L) *R59B10-Gal4* (R4m; BUa to EBoc).

(M–P) *R84H09-Gal4* (R3; BUi to EBic/ip).

(P–R) Horizontal confocal z projections of Gal4 drivers labeling columnar elements. (P and Q) *R60D05-Gal4* labels PB-EB-gall (“wedge”) neurons.

(P) Z projection depicting the complete projection pattern of the population in the CX.

(Q) Section through the EB canal is shown; “wedge” neurons most densely occupy posterior EB domains but diffusely project into intermediate and anterior domains as well.

under the control of *R88A06-Gal4*, which predominantly labels TuBu_s, the superior bulb-innervating neurons of DALCl1 (Figures 3D–3F and 4B). Quiescent flies were placed in front of a curved visual display of LEDs and presented with different visual stimuli (Figure 5A) while conducting two-photon calcium imaging from the microglomerular axonal outputs of these neurons (Figure 5B). Recordings were conducted in two planes to maximally detect microglomerular activity (see Supplemental Experimental Procedures). Responsive superior bulb microglomeruli from both planes exhibited qualitatively homogeneous characteristics and were therefore analyzed collectively, in contrast to inferior bulb microglomeruli (see below).

Receptive field mapping with a small bright (ON) object revealed that TuBu_s outputs in the superior bulb each exhibit small,

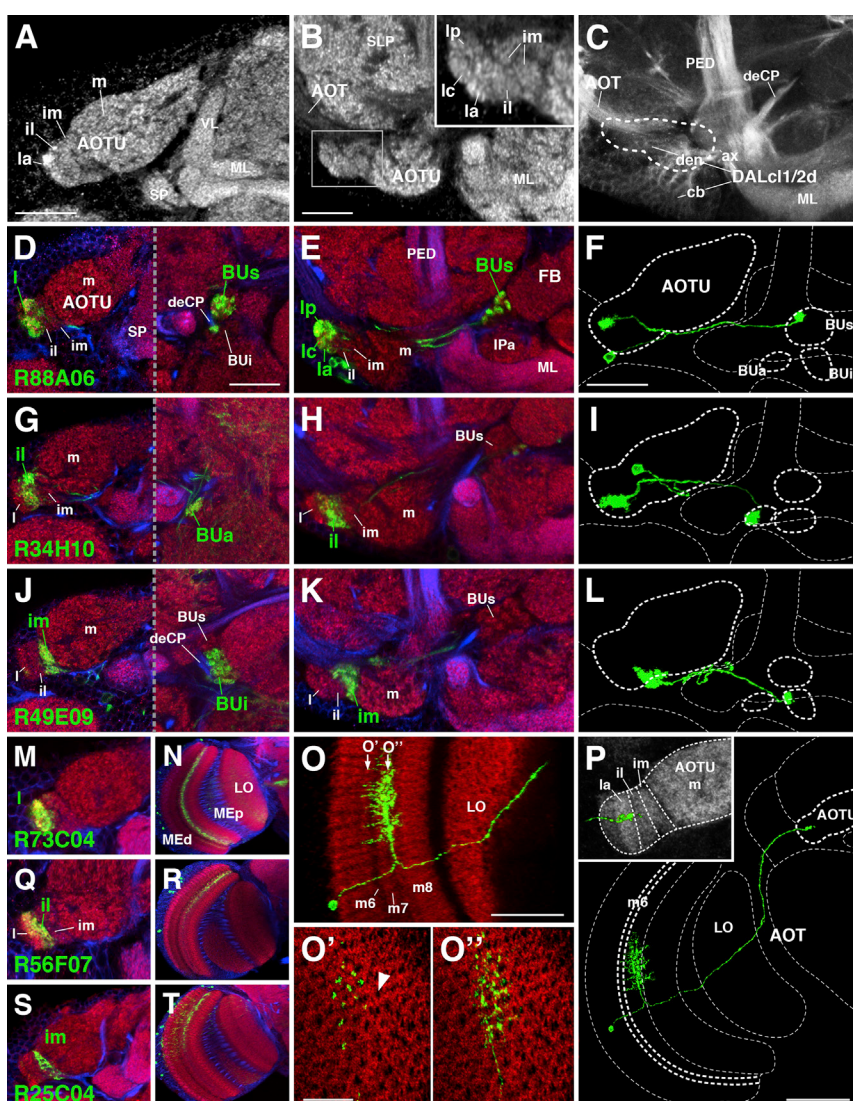


Figure 3. Topology and Architecture of TuBu and Medullo-Tubercular Neurons

(A–C) High-magnification frontal (A) and horizontal (B and C) z projections of the anterior optic tubercle reveals six distinct domains in the AOTU (ii, intermediate lateral; im, intermediate medial; la/c/p, lateral anterior/central/posterior; m, medial), highlighted by boxed inset in (B). Neuropil labeled by anti-DN-cadherin (gray; A and B) axon tracts labeled by anti-neuroglian (gray; C) with AOTU location denoted by white hatched line with locations of DALc1/2d cell bodies (cb), dendrites (den), and axons (ax).

(D–L) Gal4 drivers that label distinct TuBu neuron subclasses defined by topology within the AOTU and BU. Each row represents a distinct Gal4 driver; first and second columns are frontal and horizontal sections labeled with $10xUAS-mCD8::GFP$, respectively. Neuropil labeled with anti-DN-cadherin (red) and axon tracts by anti-Neuroglian (blue) is shown. Third column is a single-cell clone generated by MCFO using the same Gal4; white hatched lines outline neuropil compartments from the same fly.

(D–F) R88A06-Gal4 (AOTUiLa/c/p to BUs).

(G–I) R34H10-Gal4 (AOTUi to BUi).

(J–L) R49E09-Gal4 (AOTUiM to BUi).

(M–T) Gal4 drivers that label distinct medullo-tubercular neuron subclasses defined by topology within the medulla and AOTU. (M–P) R73C04-Gal4 labels a class of medullo-tubercular neurons projecting from m7 layer of the medulla to AOTUi.

(M and N) High-magnification image of the AOTU (M); (N) is the medulla from the same fly. Neuropil labeled with anti-DN-cadherin (red) and axon tracts by anti-Neuroglian (blue) is shown.

(O and P) Single-cell clone generated by MCFO with R73C04-Gal4; all panels are the same clone. Frontal section of the dendritic arborization (O) demonstrates that this cell type is not restricted to a single medulla layer. Successive tangential sections (O' and O'') reveal that the primary dendritic arborization (O') extends multiple distal processes that occupy individual medulla

columns. Neuropil labeled with anti-Brp (O–O''; red) is shown; white hatched lines outline neuropil compartments (P).

(Q and R) R56F07-Gal4 (dorsal half m7 layer to AOTUiL).

(S and T) R25C04-Gal4 (dorsal half m7 layer to AOTUiM).

AOT, anterior optic tract; deCP, central descending protocerebral fascicle; FB, fan shaped body; IPa, anterior inferior protocerebrum; IPm, medial inferior protocerebrum; LAL, lateral accessory lobe; LO, lobula; MED, distal medulla; MEp, proximal medulla; ML, medial lobe of the mushroom body; PED, peduncle of the mushroom body; SLP, superior lateral protocerebrum; SP, spur of the mushroom body. The scale bars represent 25 μ m (A), 25 μ m (B–E, G, H, J, K, M, Q, and S), 25 μ m (F, I, and L), 50 μ m (N, R, and T), 50 μ m (O), 20 μ m (O' and O''), and 50 μ m (P).

retinotopically organized receptive fields that are localized to, and provide wide coverage of, the ipsilateral visual hemifield (Figures 5C and 5D). The average receptive field size was 29.2° and 44.2° ($\pm 3.5^\circ$ and $\pm 2.8^\circ$ SD minor axis and major axis lengths, respectively; Figure 5E). The relative positioning of individual microglomeruli roughly corresponds to the positioning of the spatial receptive fields along the animal's visual elevation (Figures 5F and 5G, top panels) and azimuth (Figures 5F and 5G, bottom panels). In other words, microglomeruli with receptive fields located on the lower part of the visual field cluster in the ventrolateral part of the superior bulb, whereas microglomeruli located in the dorsomedial portion of the superior bulb have receptive fields located on the upper part of the visual field (Fig-

ures 5F and 5G). Similarly, medially located microglomeruli tend to respond to visual stimulation on the medial portion of the ipsilateral visual field, whereas laterally located microglomeruli respond on the lateral portion of it (Figures 5F and 5G). Spatial receptive fields of individual presynaptic microglomeruli were similar in size within and between animals (Figure 5E).

As R neuron dendrites are tuned to vertically oriented features, we next presented a horizontally moving bar spanning the full vertical extent of the display. Responses to a moving bright (ON) bar on a dark background are much larger by comparison to OFF bar response, indicating that TuBu_s neurons, like their downstream R neurons, are ON selective (Figure 5H) [17]. As a population, TuBu_s neurons respond maximally to a small ON

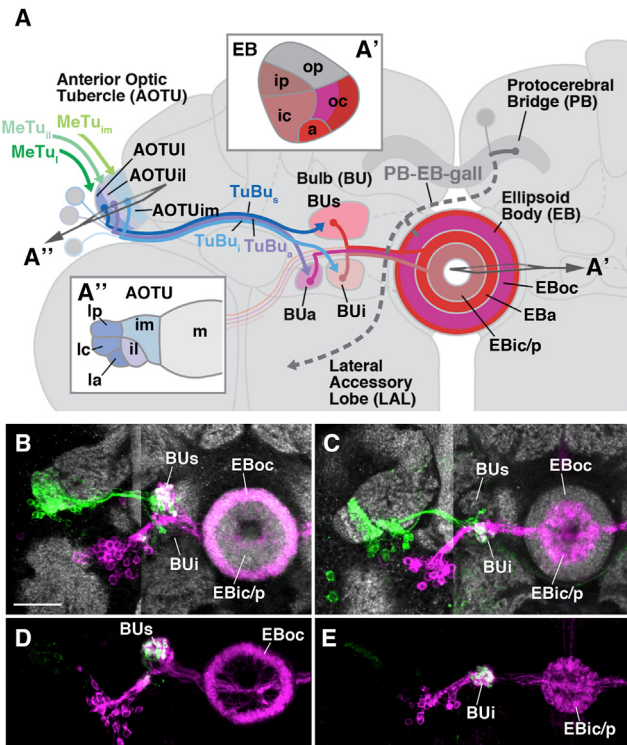


Figure 4. Framework of Connectivity in the AVP–DALcl1 and DALcl2 Provide Direct, Topographically Organized Parallel Input to R Neuron Subclasses

(A) Schematic overview of the anterior visual pathway. Insets depict horizontal sections of the EB (A') and AOTU (A'').

(B and C) Two-color labeling of superior bulb (B) and inferior bulb (C) components. TuBu neurons labeled in green by Gal4; R neurons labeled in magenta by LexA.

(B) R88A06-Gal4 labels DALcl1d TuBu neurons and R19C08-LexA labels EBoc R2 neurons; overlap is observed in the superior bulb (BUs).

(C) R49E09-Gal4 labels DALcl2d TuBu neurons and R54B05-LexA labels EBic/ip R3 neurons; overlap is observed in the inferior bulb (BUI).

(D and E) GRASP analysis of TuBu neuron–R neuron synapses using the same driver combinations as (B) and (C); postsynaptic cells are expressing CD2-RFP and split-GFP11 and presynaptic cells expressing split-GFP1-10. Strong GRASP signal is observed in the expected bulb subdomain.

The scale bars represent 25 μ m (B–E).

object, slightly less to a bar, and much less to a wide-field grating (Figure 5I). These results might suggest that TuBu_s neurons respond best to objects that fill the excitatory receptive field. Presentation of the ON object outside the excitatory receptive field did not generate measurable decreases in calcium accumulation (Figure 5J), suggesting that surround inhibition is weak if present at all. Taken together, the response properties of TuBu_s neuron presynaptic terminals resemble those of superior bulb-associated R neuron dendrites from previous reports [17], corroborating their role as direct presynaptic inputs.

We hypothesized that, due to their distinct developmental origin, DALcl2-derived TuBu_i neurons, which innervate the inferior bulb, should exhibit functional dissimilarity to superior bulb innervating, DALcl1 TuBu_s neurons (Figures 1C–1E). Flies expressing GCAMP6m under the control of the predominantly TuBu_i neuron driver, R49E09-Gal4, were presented with the

same battery of visual stimuli as shown for TuBu_s neuron microglomeruli. Unlike superior bulb TuBu_s neurons, responses in the inferior bulb TuBu_i neurons were heterogeneous and variable (see *Supplemental Experimental Procedures*; Figure S2), yet we identified one consistent response type for at least one microglomerulus in both imaging planes for every fly (Figures 6A and 6C). The receptive fields scanned in the first imaging plane typically showed excitation to objects in the contralateral visual hemifield and inhibition when the object entered the ipsilateral visual hemifield (Figures 6B and 6D, mint green). TuBu_i microglomeruli showed peculiar secondary excitation as the object left the ipsilateral visual field, at which time no visual stimulation was present (Figures 6B, black arrows, and 6D, mint green, black arrows). Qualitatively similar responses were observed from microglomeruli in the second imaging plane (Figure 6C), yet these responses were smaller in amplitude (Figure 6D, orange). In addition, we observed microglomerular structures that did not respond to any of our stimuli (Figure 6C, microglomeruli that are not encircled orange).

TuBu_i responses were asymmetric with respect to stimulus motion direction. When an object moved from the ipsilateral visual hemifield toward the contralateral one, microglomeruli responded by slight excitation followed by inhibition (Figure 6D'). We observed a strong response as the object entered the contralateral visual field (Figure 6D'). Inferior bulb response characteristics were consistent across 104 microglomeruli in 15 flies (Figures 6E and 6E'), and they were distinct from superior bulb responses. In contrast to the superior bulb, the physiological responses of R neurons that extend dendrites into the inferior bulb (R3) have not been systematically characterized, preventing us from making direct input-output comparisons. Nevertheless, the optophysiological analysis of separate TuBu neuron populations derived from DALcl1 and DALcl2 confirm the notion that different lineages form functionally distinct neuronal ensembles.

In addition to the distinct temporal dynamics of inferior and superior bulb TuBu neuron object responses, we noted that the inferior bulb microglomeruli have larger spatial receptive fields that cover the entire contralateral visual hemifield and are very similar across microglomeruli, showing strongest responses to visual stimuli presented on the upper portion of the display (Figure 6B) or after the stimulus left the screen. Whereas the spatial receptive fields and temporal response properties are distinct between superior bulb and inferior bulb, the preference for ON objects is similar (Figure 6F). Also, like superior bulb TuBu_s neurons, the inferior bulb TuBu_i neurons respond very weakly to wide-field gratings by comparison to small objects or bars (Figure 6G, see above). Our results indicate that both superior and inferior bulb-innervating TuBu neurons are sensitive to bright objects but sample unique hemifields, ipsilateral and contralateral fields, respectively, with distinct receptive field structure and temporal dynamics.

DISCUSSION

The AVP described in this work serves to define the architecture of a circuit that projects from peripheral neuronal elements of the medulla to the EB neurons of the *Drosophila* CX sequentially via MeTu neurons and parallel superior DALcl1 and inferior DALcl2 pathways (TuBu_s and TuBu_i neurons). The CX plays a pivotal role in innate and learned visually guided behaviors.

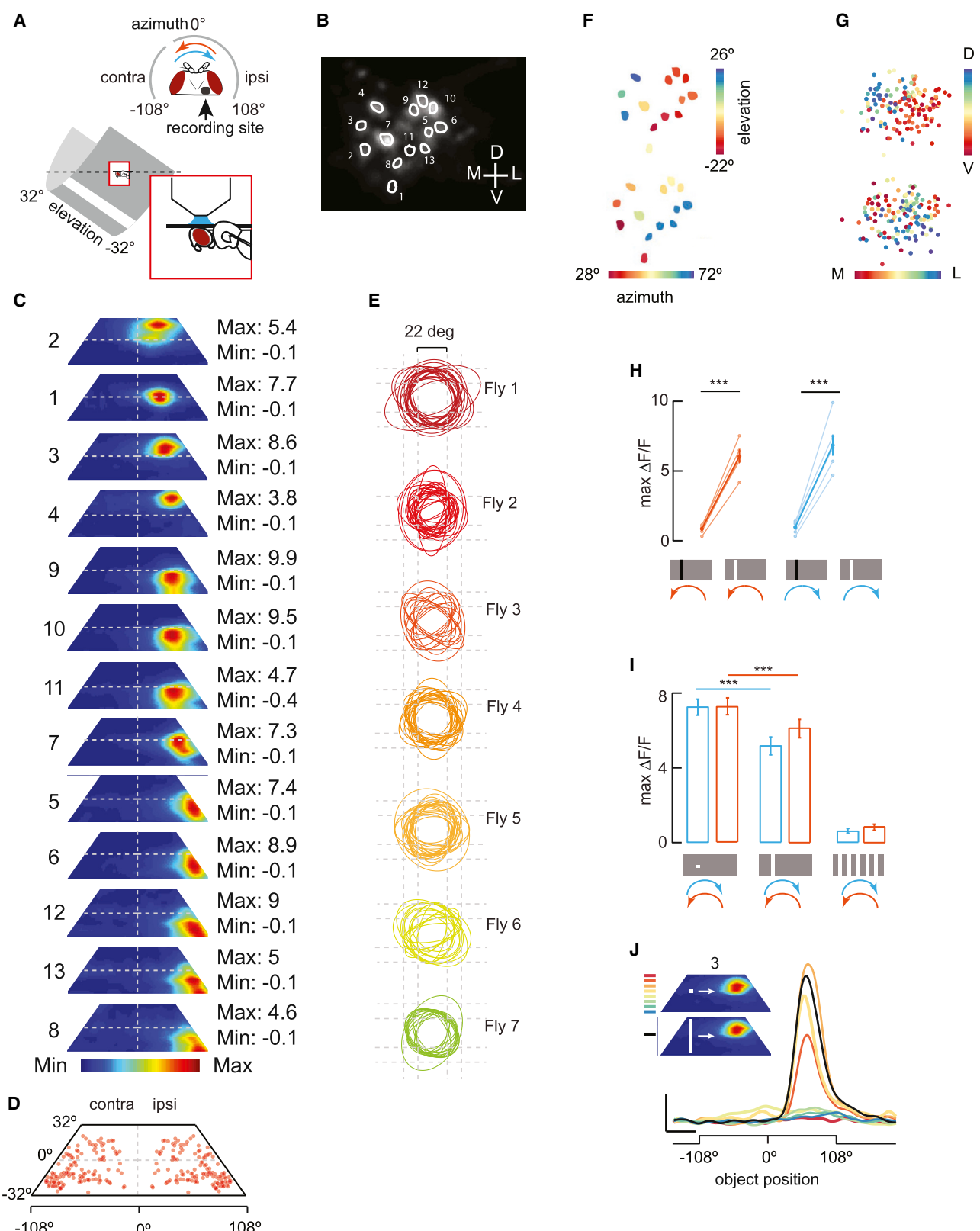


Figure 5. Physiological Properties of TuBu Neurons Innervating the Superior Bulb

(A) Schematic of two-photon experimental setup. Quiescent female flies are spatially fixed in front of a curved array of LEDs. The upper corners of the LED display are obscured by the mounting stage and outside the field of view (dashed line), which is reflected in the parallelogram receptive field projections in (C) and (D) below.

(legend continued on next page)

Recent studies by Seelig and Jayaraman [10, 17] examined the physiological responses of neuronal subpopulations within the EB. They first observed that individual R neurons whose dendritic microglomeruli are localized in the superior bulb (R2 and R4d) respond to visual stimuli. Here, we identify the developmentally related TuBu_s neurons of DALcl1 as the direct presynaptic inputs to these superior bulb R neurons and demonstrate that many of their visual tuning properties can already be observed in the upstream TuBu_s population (Figure 5). In addition, we identify DALcl2-derived TuBu_i neurons, which exhibit distinct receptive field properties from TuBu_s neurons (Figure 6) and likely supply the inferior bulb R neurons (presumably R3 neurons of the EBic domain) that have not been systematically characterized previously. TuBu_i neurons' unique receptive field and response properties suggest input from contralaterally located neurons. Indeed, neurons innervating the AOTU on both sides, described in other insects, may account for the visual interhemispheric receptive field characteristics described here and in other neurons of the sky-compass pathway [39–41].

R neurons, whose axons cover the entire perimeter of the ellipsoid body, provide input to the large number of columnar neurons (so-called "wedge neurons") [33], the neurites of which subdivide the torus-shaped volume of the ellipsoid body into narrow radial partitions. The calcium dynamics recorded from the population of wedge neurons produces a localized "bump" of activity in the torus, which, based on visual landmarks and proprioception, corresponds to an internal representation of the animal's orientation in space [10]. Information likely reverberates between the EB and other CX neuropils, such as the protocerebral bridge, via different populations of columnar elements (wedge and tile neurons), which heavily interconnect them [33]. Similarly to the head direction system in mammalian brains, these dynamics produce stable neural activity consistent with an internal compass [10]. The EB displays a common organizational principle observed in complex nervous systems; in essence, it is a structure arranged into layers and columns by tangential (R neurons) and columnar

(wedge and tile neurons) elements, respectively. A receptive field-specific response in a single R neuron would presumably influence activity in an entire layer and thus all columns. One of the most insightful lines of inquiry will be to investigate how this tangential input is translated into (or is even compatible with) the localized columnar activity ("bump") within the wedge neurons of the EB. It is conceivable that R neurons, due to their peculiar bifurcated architecture, may influence EB wedges with a physiologically relevant temporal offset, which could be utilized to modulate spatially restricted activity patterns. Future work defining the circuit motifs present in this brain region may provide insight into the advantages of a layered and columnar organization for emergent neural properties, such as a cognitive-like internal representation and navigation.

The neurons and neuropil compartments of the *Drosophila* AVP have homologous counterparts in other insects, forming the so-called "sky-compass pathway" most prominently investigated in the locust (*Schistocerca gregaria*) [18, 39, 42], monarch butterfly (*Danaus plexippus*) [43], honeybee (*Apis mellifera*) [22], and bumblebee (*Bombus ignites*) [21]. MeTu neurons providing input to the AVP form dendritic branches within the boundary region of distal and proximal medulla [21, 22, 44]. The target neuropil innervated by MeTu neurons is the lateral/intermediate part of the AOTU, called the "lower unit or lower unit complex" of the AOTU (AOTU-LU or LUC) in locust and other insects [1, 39, 45]. Two classes of neurons, TuLAL1a and TuLAL1b, likely counterparts of the TuBu neurons described in this paper, form two parallel pathways that convey the output from the AOTU-LUC to small neuropil foci within the LAL, which are homologous to the bulb, formerly called the lateral triangle and median olive. From here, TL neurons, homologs of fly R neurons, carry the visual input to the lower unit of the central body, counterpart of the *Drosophila* ellipsoid body [18]. Based on the available anatomical and functional data, it is not yet possible to propose more specific homologies between neuron classes of the AVP in flies and the corresponding sky compass pathway in other insects.

- (B) Two-photon excitation image of a representative fly in which R88A06-Gal4 is driving the expression of GCaMP6m in DALcl1-derived tubercular-bulbar neurons of the superior bulb (TuBu_s). All recordings are from the microglomerular presynaptic terminals of the right bulb. Responsive microglomeruli are randomly indicated numerically as individual regions of interest (ROIs) (white).
- (C) For individual microglomeruli enumerated from representative fly in (B), receptive field maps were generated using a small object passed at eight different elevation trajectories in both directions. Maps from 13 microglomeruli are sorted from highest to lowest elevation center of the receptive field "hotspot" to indicate the visual coverage by an ensemble of receptive fields. All receptive fields are mapped from ipsilateral microglomeruli. See also Figure S1.
- (D) The locations of receptive field centers from all receptive field measurements (136 ROIs) from all flies (n = 7) are indicated with red dots, demonstrating the coverage across the visual field. To facilitate visual comparison, receptive field centers measured from ipsilateral ROIs are reflected to the contralateral side under the presumptions of bilateral symmetry.
- (E) Circumference tracings of receptive fields measured from seven flies, 136 ROIs, demonstrate stereotypy of receptive field size across microglomeruli and across animals.
- (F) The spatial arrangement of imaged microglomeruli ROIs recorded from a single fly (ROIs from B) are color coded according to receptive field location in elevation (top) and azimuth (bottom) to indicate retinotopic arrangement.
- (G) Similar to (F), the retinotopic distribution of microglomeruli recorded from all seven flies and 136 microglomeruli ROIs. Each microglomerular ROI is indicated by a small uniform dot color coded as in (F). D, V, M, and L indicate dorsal, ventral, medial, and lateral.
- (H and I) Visual stimuli presented in both horizontal directions as shown in (A); ipsi-to-contra motion (orange) and contra-to-ipsi motion (blue).
- (H) Pairwise comparison between the mean of maximum ΔF/F responses from all ROIs and all preparations to both an OFF and ON bar n = 7 (p < 0.001; Wilcoxon signed rank test).
- (I) Mean of pooled peak amplitude responses relative to stimulus onset from six flies to an ON object (left), an ON bar (middle), and a wide-field grating (right). n = 6. Error bars indicate SEM; p < 0.001; Wilcoxon signed rank test.
- (J) Superior bulb microglomeruli do not show surround inhibition. From a single representative ROI (microglomerulus 3 from B), calcium responses are shown for eight different trajectories of an ON object (color indicates elevation of horizontal sweep) by comparison to an ON bar spanning the full elevation of the display (black trace). The bar evokes nearly the same response as the object passing through the hotspot of the receptive field. The scale bar represents 200% ΔF/F and 2 s, y and x axis, respectively.

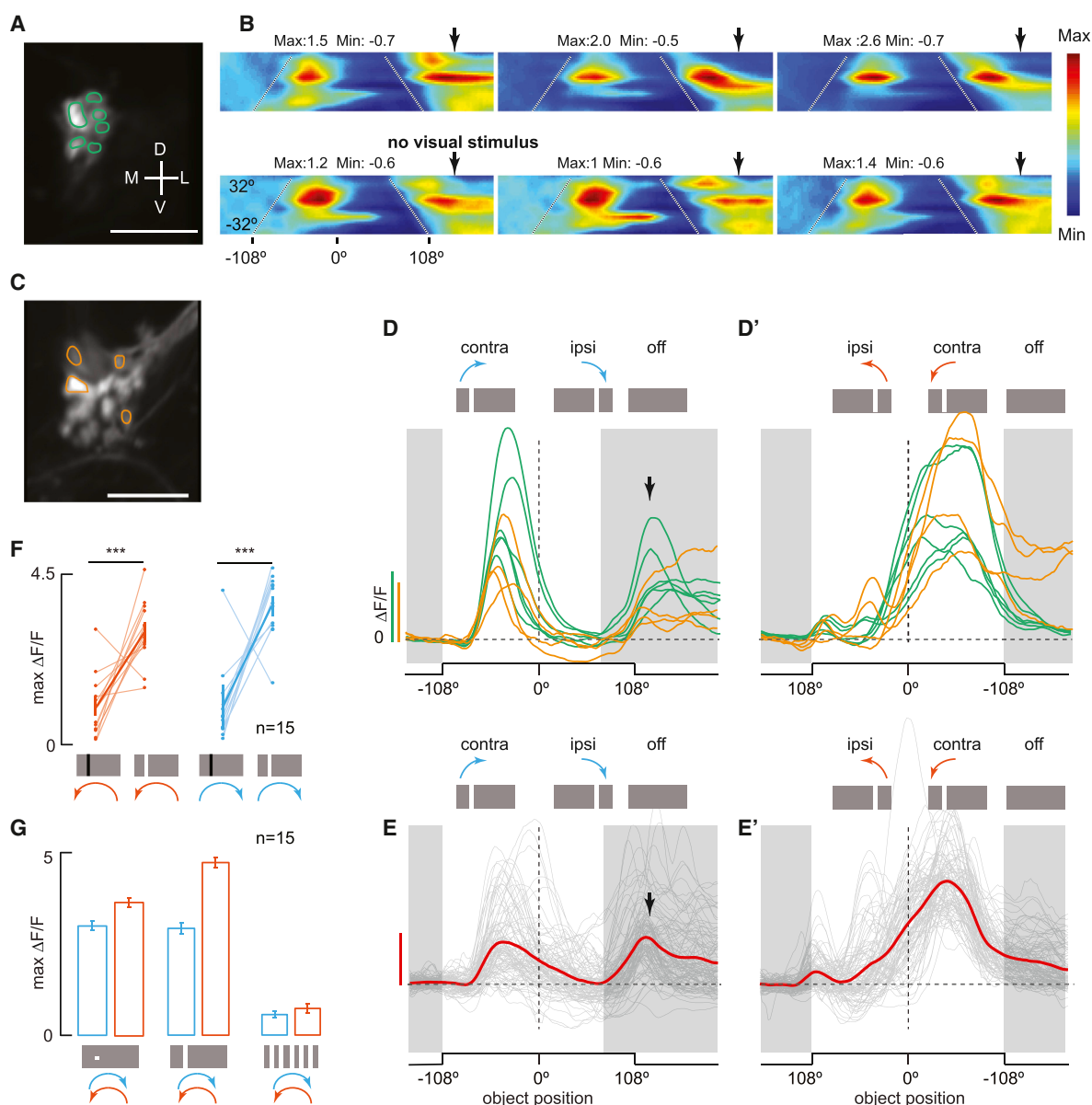


Figure 6. Physiological Properties of TuBu Neurons Innervating the Inferior Bulb

(A–E') Canonical responses from a subset of inferior bulb microglomeruli.

(A) Two-photon excitation image of a representative fly in which R49E09-Ga4 is driving the expression of GCaMP6m in DALcl2 tubercular-bulbar neurons of the inferior bulb (TuBu). Imaging plane reflects the microglomeruli (ROIs; mint green) in the dorso-posterior-most position in the inferior bulb.

(B) Receptive field maps of ROIs in (A) generated by contralateral to ipsilateral (contra-to-ipsi) motion of an ON object passed at eight different elevation trajectories. Maps demonstrate stereotypy of a class of microglomeruli typically localized to this position in the inferior bulb. Receptive fields are large and centered in the contralateral visual hemifield. Calcium accumulation decreases for stimuli in the ipsilateral visual field as indicated by negative minimum $\Delta F/F$ values. Note secondary excitation after the object has left the field of view (black arrows). White dashed lines indicate display boundaries.

(C) Second imaging plane from same preparation as (A) contains some microglomeruli that exhibit a canonical TuBu_i response (light orange) but also many that do not (unlabeled microglomeruli).

(D and D') ON bar responses from inferior bulb microglomeruli that exhibit the canonical response described in (B) from the representative fly shown in (A)–(C). Responses from ROIs from the first plane (mint green) and second plane (light orange) are shown as traces from contra-to-ipsi presentation (D) and ipsilateral to contralateral (ipsi-to-contra) presentation (D') of the ON bar. Scale bars are 400% $\Delta F/F$ for mint green and 100% $\Delta F/F$ for light orange. Shaded gray envelopes indicate portions of the experiment when the stimulus is out of the visual field. Black arrow indicates secondary microglomeruli responses after the ON bar has left the visual field. See also Figure S2.

(E and E') Pooled population data from all ROIs and all flies, exhibiting on average distinct TuBu_i response for contra-to-ipsi (E) and ipsi-to-contra (E') presentation of the ON bar. Raw traces are shown in gray and mean of all traces in red. The scale bar represents 200% $\Delta F/F$. Shaded gray envelopes and black arrow are as described in (D) and (D'). n = 15; 104 ROIs.

(F and G) Visual stimuli presented in both horizontal directions; ipsi-to-contra motion (blue) and contra-to-ipsi motion (orange).

(legend continued on next page)

Most notably recognized as the polarization (POL) vision pathway, neurons of the sky-compass network are tuned to the e-vectors of polarized light, which reflect the location of the sun, thus providing compass information used by these insects to navigate during long-range migrations or local path integration in central place foraging [43, 46]. Considering that *Drosophila* also exhibits physiological and behavioral correlates with POL sensitivity [47–49], we posit that the fly AVP is the neural circuit for POL information transmission to the CX. However, a recent report demonstrated that when flies are presented with a rotating field of polarized UV light in conjunction with pan-neuronal calcium imaging, robust calcium signals in any CX neuropils, including the bulb, were not observed [50]. In contrast, and in agreement with our findings, bright objects elicited strong responses in the bulb and other regions of the CX. Indeed, neurons of the sky-compass pathway can encode both a specific e-vector and the azimuthal position of an unpolarized light source, the nature and degree of which depend on the insect and neuron type in question [24, 41–43]. The extent of encoding strength to a given stimulus (polarized versus unpolarized light) likely reflects the ethology and ecological niche of the animal. For example, diurnal dung beetles utilize the position of a bright object (such as the sun or moon) to navigate regardless of ambient light intensity, whereas nocturnal beetles utilize polarized skylight specifically at low light intensities rather than position of a celestial body, such as the moon. This ethological distinction is reflected in the tuning properties of neurons within the sky-compass pathway, even between two closely related insects [24].

In the *Drosophila* AVP, the spatial position of luminance cues emanating from a bright source, such as a celestial body or an escape route from within foliage, would be represented more strongly than the skylight pattern of polarized light [50]. This proposition is based on the following:

- (1) Anatomical and ethological evidence: in comparison to other insects examined, in which an aspect of their behavioral repertoire is thought to depend on POL vision, the ethological lifestyle of *Drosophila* suggests that it may be less likely to use the pattern of polarized skylight to navigate. This fact is reflected in their relatively rudimentary dorsal rim area (DRA), a region of the eye with specialized, POL-sensitive photoreceptors, and correspondingly inconspicuous dorsal rim area of the medulla (MEDRA), which receives input from DRA photoreceptors. In addition, likely homologs of MeTu neurons in other insects (transmedulla neurons) often exhibit long, dorsally projecting input neurites, which ramify in the MEDRA, suggesting a high degree of POL input [21, 22]. In contrast, we did not observe this characteristic feature in MeTu neurons in *Drosophila*; dendritic arborizations ramified locally of the primary neurite, which were distributed relatively evenly throughout the dorsal half of or the whole eye.
- (2) Upstream TuBu as well as downstream R neurons and wedge neurons show strong excitation to bright objects

[10, 17], whereas dark object responses are weaker (Figures 5 and 6), suggesting specialization for detecting a bright object against a dark background. The ON preference and weak tuning to object size by TuBu neurons (Figures 5 and 6) suggest that this pathway would poorly mediate stripe fixation behavior, which is activated more by dark bars or complex motion-defined edges [51]. However, the topographical organization of TuBu_s neuron terminals (Figure 5) suggests that retinotopy is conserved and thus could serve spatial navigation, unlike other small-object visual projection neurons (VPNs) of the lobula and lobula plate, where the retinotopy is apparently lost within the intermingled axon terminals of individual small-field columnar neurons [52, 53].

- (3) The preference for bright objects of varying size suggests that the CX receives rather primitive spatial information by comparison to the complex filtering properties exhibited by other VPN pathways that act as precise spatial filters for directional patterns of optic flow, the spatial dynamics of looming objects, and the omni-directional motion of small OFF-contrasting objects [52–54].
- (4) Spatial interactions of excitation and inhibition: a single bright object presented ipsilaterally against a dark background would excite a spatially defined subset of ipsilateral TuBu_s neurons while simultaneously exciting multiple (possibly all) canonical contralateral TuBu_i neurons. By contrast, two bright spots appearing in the left and right visual fields would simultaneously stimulate TuBu_s neurons on both right and left side while leading to inhibition in all TuBu_i neurons. Most intriguingly, TuBu_i neurons show strong calcium currents as a bright object leaves the visual field, suggesting that TuBu_i neurons might be signaling to the R neurons some crucial information about “losing” the visual bearing to a bright object. R neurons have shown to be indispensable for visual place learning [8], and it is possible that inferior bulb neurons have a crucial role in carrying some of the visual information that is used by R neurons to mediate this behavior.

Here, we provide ample evidence that DALc1- and DALc12-derived neurons have unique functional properties, come from distinct lineages, and supply visual information to the central complex. To our knowledge, this is the first extensive characterization of the visual input to the central complex in *Drosophila* and a definitive example of how developmentally distinct lineages give rise to functionally distinct circuits.

EXPERIMENTAL PROCEDURES

Drosophila Stocks

Flies were reared at 25°C using standard fly media unless otherwise noted. The *Drosophila* driver lines utilized in this study, as well as more specific genotype information, are listed in the [Supplemental Experimental Procedures](#). The

(F) Pairwise comparison between the mean of maximum ΔF/F responses from all ROIs that exhibit a canonical TuBu_i response from each preparation, indicating ON selectivity ($n = 15$; $p < 0.001$; Wilcoxon signed rank test).

(G) Mean of pooled peak amplitude responses relative to stimulus onset from 15 flies to an ON object (left), an ON bar (middle), and wide-field gratings (right). $n = 15$; error bars indicate SEM.

following general transgenic fly stocks were used: *UAS-DenMark::mCherry*; *UAS-Syt::GFP*; *su(Hw)attP8:HA_V5_FLAG_1* [31]; *10xUAS-mCD8::GFP*; *10XUAS-IVS-mCD8::RFP*; *13XLexAop2-mCD8::GFP*; *LexAop-CD2::RFP*; *UAS-CD4::spGFP1-10*; *LexAop-CD4::spGFP11*; and *20xUAS-GCAMP6m* (Bloomington Stock Center).

Clonal Analysis

GFP-labeled adult neuroblast MARCM clones were induced at the late first instar/early second instar stage by heat shocking in a water bath at 38°C for 30–60 min. Larvae were approximately 12–44 hr old. Heat-shocked larvae were grown to adult for analysis.

Single-cell analysis of neurons in the AVP pathway was conducted using the MCFO method described previously [31, 33]. Briefly, depending on the cell density of a given Gal4 line, 1- to 3-day-old flies were dissected to obtain single-cell labeling.

Immunostaining, Confocal Microscopy, and Image Analysis

Immunohistochemistry was performed using standard procedures with some modifications [26]; details for staining procedures and list of antibodies are in *Supplemental Experimental Procedures*. *Drosophila* adult brains labeled with antibody markers were viewed as whole mounts in Vectashield mounting medium H-1000 (Vector Laboratories) by confocal microscopy (LSM 700 Imager M2 using Zen 2009 [Carl Zeiss]; lenses: 40× oil [numerical aperture 1.3]). Complete series of optical sections were taken from preparations between 1.2- and 2-μM intervals. Preparations were mounted anteriorly or dorsally. Dorsally oriented preparations were acquired by sliding the brain dorsal side up, inside the crevice between two closely apposed coverslips. Captured images were processed by ImageJ or FIJI (NIH; <http://rsbweb.nih.gov/ij/> and <http://fiji.sc/>). In Figures 1B–1G, background labeling was manually removed to improve clarity of specific neuronal morphologies. In Figure 1E, ventral hemilineages of DALcl1/2 were digitally removed, and z projections of the labeled dorsal hemilineages were registered digitally with z projections of a standard brain at the corresponding antero-posterior plane using the scaling and warping tool in the NIH ImageJ and Adobe Photoshop software programs. Easily recognizable landmarks, including the center of the peduncle and ellipsoid body, and the tips of the mushroom body lobes were used as fiduciary points. For multicolor flip-out experiments, additional non-overlapping neurons were manually removed and anti-Brp-labeled neuropil compartments were outlined with hatched lines from the same sample. Schematics were made in Adobe Illustrator and figures assembled in Adobe Photoshop.

Two-Photon Calcium Imaging, Visual Stimuli, and Two-Photon Imaging Analysis

Calcium imaging was conducted as previously described [53]. Briefly, calcium-dependent fluorescent signals were detected using a two-photon excitation scanning microscope (3i) with Slidebook 6 software (3i) at an image acquisition rate of 10 frames/s. Three- to seven-day-old female flies expressing *20xUAS-GCAMP6m* under the control of a specific Gal4 driver labeling TuBu neuron subpopulations were used; all recordings were conducted from the microglomerular presynaptic terminals of these neurons. Flies were immobilized in a custom holder and bathed in physiological saline; neurons of interest were made optically accessible by dissecting the posterior cuticle of the head capsule. Visual stimuli were presented to the fly using a 96 × 32 pixel LED arena. Specific details of two-photon imaging setup, visual stimuli, and imaging analysis are provided in *Supplemental Experimental Procedures*.

SUPPLEMENTAL INFORMATION

Supplemental Information includes two figures and Supplemental Experimental Procedures and can be found with this article online at <http://dx.doi.org/10.1016/j.cub.2017.02.063>.

AUTHOR CONTRIBUTIONS

Conceptualization, J.J.O., M.F.K., M.A.F., and V.H.; Methodology, J.J.O. and M.F.K.; Formal Analysis, M.F.K.; Investigation, J.J.O., M.F.K., B.-C.M.N., C.B., and J.K.L.; Writing – Original Draft, J.J.O., M.F.K., M.A.F., and V.H.; Visualiza-

tion, J.J.O., M.F.K., M.A.F., and V.H.; Supervision and Funding Acquisition, M.A.F. and V.H.

ACKNOWLEDGMENTS

We thank Orkun Akin for kindly sharing the image alignment algorithm. We also thank Hiroshi Shiozaki and Hokto Kazama for discussing unpublished results. This work was supported by the NIH (grants R01 NS096290 to V.H. and R01 EY026031 to M.A.F.), an NIH Ruth L. Kirschstein National Research Service Award (to J.J.O.; GM007185), the UCLA Edith Hyde Fellowship (to M.F.K.), and the University of California, Los Angeles Dissertation Year Fellowship (to J.J.O. and M.F.K.).

Received: January 19, 2017

Revised: February 24, 2017

Accepted: February 27, 2017

Published: March 30, 2017

REFERENCES

- Ito, K., Shinomiya, K., Ito, M., Armstrong, J.D., Boyan, G., Hartenstein, V., Harzsch, S., Heisenberg, M., Homberg, U., Jenett, A., et al.; Insect Brain Name Working Group (2014). A systematic nomenclature for the insect brain. *Neuron* 81, 755–765.
- Strausfeld, N.J. (1976). *Atlas of an Insect Brain* (Springer).
- Hanesch, U., Fischbach, K.-F., and Heisenberg, M. (1989). Neuronal architecture of the central complex in *Drosophila melanogaster*. *Cell Tissue Res.* 257, 343–366.
- Huber, F. (1960). Untersuchungen über die funktion des zentralnervensystems und insbesondere des gehirnes bei der fortbewegung und der lauterzeugung der grillen. Z. Vgl. Physiol. 44, 60–132.
- Otto, D. (1971). Untersuchungen zur zentralnervösen kontrolle der lauterzeugung von grillen. Z. Vgl. Physiol. 74, 227–271.
- Strauss, R., and Heisenberg, M. (1993). A higher control center of locomotor behavior in the *Drosophila* brain. *J. Neurosci.* 13, 1852–1861.
- Ilius, M., Wolf, R., and Heisenberg, M. (2007). The central complex of *Drosophila melanogaster* is involved in flight control: studies on mutants and mosaics of the gene ellipsoid body open. *J. Neurogenet.* 21, 321–338.
- Ofstad, T.A., Zuker, C.S., and Reiser, M.B. (2011). Visual place learning in *Drosophila melanogaster*. *Nature* 474, 204–207.
- Neuser, K., Triphan, T., Mronz, M., Poeck, B., and Strauss, R. (2008). Analysis of a spatial orientation memory in *Drosophila*. *Nature* 453, 1244–1247.
- Seelig, J.D., and Jayaraman, V. (2015). Neural dynamics for landmark orientation and angular path integration. *Nature* 521, 186–191.
- Poucet, B., Chaillan, F., Truchet, B., Save, E., Sargolini, F., and Hok, V. (2015). Is there a pilot in the brain? Contribution of the self-positioning system to spatial navigation. *Front. Behav. Neurosci.* 9, 292.
- Lai, S.-L., Awasaki, T., Ito, K., and Lee, T. (2008). Clonal analysis of *Drosophila* antennal lobe neurons: diverse neuronal architectures in the lateral neuroblast lineage. *Development* 135, 2883–2893.
- Das, A., Gupta, T., Davla, S., Prieto-Godino, L.L., Diegelmann, S., Reddy, O.V., Raghavan, K.V., Reichert, H., Lovick, J., and Hartenstein, V. (2013). Neuroblast lineage-specific origin of the neurons of the *Drosophila* larval olfactory system. *Dev. Biol.* 373, 322–337.
- Hartenstein, V., Spindler, S., Pereanu, W., and Fung, S. (2008). The development of the *Drosophila* larval brain. In *Brain Development in *Drosophila melanogaster**, G.M. Technau, ed. (Springer), pp. 1–31.
- Jefferis, G.S.X.E., Marin, E.C., Stocker, R.F., and Luo, L. (2001). Target neuron prespecification in the olfactory map of *Drosophila*. *Nature* 414, 204–208.
- Marin, E.C., Jefferis, G.S.X.E., Komiyama, T., Zhu, H., and Luo, L. (2002). Representation of the glomerular olfactory map in the *Drosophila* brain. *Cell* 109, 243–255.

17. Seelig, J.D., and Jayaraman, V. (2013). Feature detection and orientation tuning in the *Drosophila* central complex. *Nature* 503, 262–266.
18. el Jundi, B., Pfeiffer, K., Heinze, S., and Homberg, U. (2014). Integration of polarization and chromatic cues in the insect sky compass. *J. Comp. Physiol. A Neuroethol. Sens. Neural Behav. Physiol.* 200, 575–589.
19. Träger, U., Wagner, R., Bausenwein, B., and Homberg, U. (2008). A novel type of microglomerular synaptic complex in the polarization vision pathway of the locust brain. *J. Comp. Neurol.* 506, 288–300.
20. Heinze, S., Florman, J., Asokaraj, S., El Jundi, B., and Reppert, S.M. (2013). Anatomical basis of sun compass navigation II: the neuronal composition of the central complex of the monarch butterfly. *J. Comp. Neurol.* 521, 267–298.
21. Pfeiffer, K., and Kinoshita, M. (2012). Segregation of visual inputs from different regions of the compound eye in two parallel pathways through the anterior optic tubercle of the bumblebee (*Bombus ignitus*). *J. Comp. Neurol.* 520, 212–229.
22. Zeller, M., Held, M., Bender, J., Berz, A., Heinloth, T., Hellfritz, T., and Pfeiffer, K. (2015). Transmedulla neurons in the sky compass network of the honeybee (*Apis mellifera*) are a possible site of circadian input. *PLoS ONE* 10, e0143244.
23. Held, M., Berz, A., Hensgen, R., Muenz, T.S., Scholl, C., Rössler, W., Homberg, U., and Pfeiffer, K. (2016). Microglomerular synaptic complexes in the sky-compass network of the honeybee connect parallel pathways from the anterior optic tubercle to the central complex. *Front. Behav. Neurosci.* 10, 186.
24. el Jundi, B., Warrant, E.J., Byrne, M.J., Khaldy, L., Baird, E., Smolka, J., and Dacke, M. (2015). Neural coding underlying the cue preference for celestial orientation. *Proc. Natl. Acad. Sci. USA* 112, 11395–11400.
25. Lovick, J.K., Ngo, K.T., Omoto, J.J., Wong, D.C., Nguyen, J.D., and Hartenstein, V. (2013). Postembryonic lineages of the *Drosophila* brain: I. Development of the lineage-associated fiber tracts. *Dev. Biol.* 384, 228–257.
26. Wong, D.C., Lovick, J.K., Ngo, K.T., Borisutthirattana, W., Omoto, J.J., and Hartenstein, V. (2013). Postembryonic lineages of the *Drosophila* brain: II. Identification of lineage projection patterns based on MARCM clones. *Dev. Biol.* 384, 258–289.
27. Ito, M., Masuda, N., Shinomiya, K., Endo, K., and Ito, K. (2013). Systematic analysis of neural projections reveals clonal composition of the *Drosophila* brain. *Curr. Biol.* 23, 644–655.
28. Yu, H.H., Awasaki, T., Schroeder, M.D., Long, F., Yang, J.S., He, Y., Ding, P., Kao, J.C., Wu, G.Y.Y., Peng, H., et al. (2013). Clonal development and organization of the adult *Drosophila* central brain. *Curr. Biol.* 23, 633–643.
29. Pereanu, W., Kumar, A., Jennett, A., Reichert, H., and Hartenstein, V. (2010). Development-based compartmentalization of the *Drosophila* central brain. *J. Comp. Neurol.* 518, 2996–3023.
30. Jenett, A., Rubin, G.M., Ngo, T.T.B., Shepherd, D., Murphy, C., Dionne, H., Pfeiffer, B.D., Cavallaro, A., Hall, D., Jeter, J., et al. (2012). A GAL4-driver line resource for *Drosophila* neurobiology. *Cell Rep.* 2, 991–1001.
31. Nern, A., Pfeiffer, B.D., and Rubin, G.M. (2015). Optimized tools for multi-color stochastic labeling reveal diverse stereotyped cell arrangements in the fly visual system. *Proc. Natl. Acad. Sci. USA* 112, E2967–E2976.
32. Renn, S.C., Armstrong, J.D., Yang, M., Wang, Z., An, X., Kaiser, K., and Taghert, P.H. (1999). Genetic analysis of the *Drosophila* ellipsoid body neuropil: organization and development of the central complex. *J. Neurobiol.* 41, 189–207.
33. Wolff, T., Iyer, N.A., and Rubin, G.M. (2015). Neuroarchitecture and neuroanatomy of the *Drosophila* central complex: A GAL4-based dissection of protocerebral bridge neurons and circuits. *J. Comp. Neurol.* 523, 997–1037.
34. Yang, J.S., Awasaki, T., Yu, H.-H., He, Y., Ding, P., Kao, J.-C., and Lee, T. (2013). Diverse neuronal lineages make stereotyped contributions to the *Drosophila* locomotor control center, the central complex. *J. Comp. Neurol.* 521, 2645–2662, Spc1.
35. Namiki, S., and Kanzaki, R. (2016). Comparative neuroanatomy of the lateral accessory lobe in the insect brain. *Front. Physiol.* 7, 244.
36. Otsuna, H., Shinomiya, K., and Ito, K. (2014). Parallel neural pathways in higher visual centers of the *Drosophila* brain that mediate wavelength-specific behavior. *Front. Neural Circuits* 8, 8.
37. Panser, K., Tirian, L., Schulze, F., Villalba, S., Jefferis, G.S.X.E., Bühler, K., and Straw, A.D. (2016). Automatic segmentation of *Drosophila* neural compartments using GAL4 expression data reveals novel visual pathways. *Curr. Biol.* 26, 1943–1954.
38. Fischbach, K.-F., and Dittrich, A.P.M. (1989). The optic lobe of *Drosophila melanogaster*. I: A Golgi analysis of wild-type structure. *Cell Tissue Res.* 258, 441–475.
39. Homberg, U., Hofer, S., Pfeiffer, K., and Gebhardt, S. (2003). Organization and neural connections of the anterior optic tubercle in the brain of the locust, *Schistocerca gregaria*. *J. Comp. Neurol.* 462, 415–430.
40. Heinze, S., Gotthardt, S., and Homberg, U. (2009). Transformation of polarized light information in the central complex of the locust. *J. Neurosci.* 29, 11783–11793.
41. Pfeiffer, K., and Homberg, U. (2007). Coding of azimuthal directions via time-compensated combination of celestial compass cues. *Curr. Biol.* 17, 960–965.
42. Pfeiffer, K., Kinoshita, M., and Homberg, U. (2005). Polarization-sensitive and light-sensitive neurons in two parallel pathways passing through the anterior optic tubercle in the locust brain. *J. Neurophysiol.* 94, 3903–3915.
43. Heinze, S., and Reppert, S.M. (2011). Sun compass integration of skylight cues in migratory monarch butterflies. *Neuron* 69, 345–358.
44. el Jundi, B., Pfeiffer, K., and Homberg, U. (2011). A distinct layer of the medulla integrates sky compass signals in the brain of an insect. *PLoS ONE* 6, e27855.
45. Heinze, S., and Reppert, S.M. (2012). Anatomical basis of sun compass navigation I: the general layout of the monarch butterfly brain. *J. Comp. Neurol.* 520, 1599–1628.
46. Homberg, U., Heinze, S., Pfeiffer, K., Kinoshita, M., and el Jundi, B. (2011). Central neural coding of sky polarization in insects. *Philos. Trans. R. Soc. Lond. B Biol. Sci.* 366, 680–687.
47. Weir, P.T., and Dickinson, M.H. (2012). Flying *Drosophila* orient to sky polarization. *Curr. Biol.* 22, 21–27.
48. Wernet, M.F., Velez, M.M., Clark, D.A., Baumann-Klausener, F., Brown, J.R., Klovstad, M., Labhart, T., and Clandinin, T.R. (2012). Genetic dissection reveals two separate retinal substrates for polarization vision in *Drosophila*. *Curr. Biol.* 22, 12–20.
49. Weir, P.T., Henze, M.J., Bleul, C., Baumann-Klausener, F., Labhart, T., and Dickinson, M.H. (2016). Anatomical reconstruction and functional imaging reveal an ordered array of skylight polarization detectors in *Drosophila*. *J. Neurosci.* 36, 5397–5404.
50. Weir, P.T., and Dickinson, M.H. (2015). Functional divisions for visual processing in the central brain of flying *Drosophila*. *Proc. Natl. Acad. Sci. USA* 112, E5523–E5532.
51. Maimon, G., Straw, A.D., and Dickinson, M.H. (2008). A simple vision-based algorithm for decision making in flying *Drosophila*. *Curr. Biol.* 18, 464–470.
52. Wu, M., Nern, A., Williamson, W.R., Morimoto, M.M., Reiser, M.B., Card, G.M., and Rubin, G.M. (2016). Visual projection neurons in the *Drosophila* lobula link feature detection to distinct behavioral programs. *eLife* 5, e21022.
53. Keles, M.F., and Frye, M.A. (2017). Object-detecting neurons in *Drosophila*. *Curr. Biol.* Published online February 9, 2017. <http://dx.doi.org/10.1016/j.cub.2017.01.012>.
54. Maisak, M.S., Haag, J., Ammer, G., Serbe, E., Meier, M., Leonhardt, A., Schilling, T., Bahl, A., Rubin, G.M., Nern, A., et al. (2013). A directional tuning map of *Drosophila* elementary motion detectors. *Nature* 500, 212–216.